Mon. Not. R. Astron. Soc. **000**, 1–17 (2013) Printed 31 May 2013 (MN LATEX style file v2.2)

A discontinuous Galerkin method for solving the fluid and MHD equations in astrophysical simulations

Philip Mocz[1⋆], Mark Vogelsberger[1]†, Debora Sijacki[1,2], Rüdiger Pakmor[3], and Lars Hernquist[1]
[1]*Harvard University, Cambridge, MA 02138, USA*
[2]*Kavli Institute for Cosmology, Cambridge and Institute of Astronomy, Madingley Road, Cambridge, CB3 0HA*
[3]*Heidelberger Institut für Theoretische Studien, Schloss-Wolfsbrunnenweg 35, 69118 Heidelberg, Germany*

subm. to MNRAS, xx xxx 2013

ABSTRACT

A discontinuous Galerkin (DG) method suitable for large-scale astrophysical simulations on Cartesian meshes as well as arbitrary static and moving Voronoi meshes is presented. Most major astrophysical fluid dynamics codes use a finite volume (FV) approach. We demonstrate that the DG technique offers distinct advantages over FV formulations on both static and moving meshes. The DG method is also easily generalized to higher than second-order accuracy without requiring the use of extended stencils to estimate derivatives (thereby making the scheme highly parallelizable). We implement the technique in the AREPO code for solving the fluid and the magnetohydrodynamic (MHD) equations. By examining various test problems, we show that our new formulation provides improved accuracy over FV approaches of the same order, and reduces post-shock oscillations and artificial diffusion of angular momentum. In addition, the DG method makes it possible to represent magnetic fields in a locally divergence-free way, improving the stability of MHD simulations and moderating global divergence errors, and is a viable alternative for solving the MHD equations on meshes where Constrained-Transport (CT) cannot be applied. We find that the DG procedure on a moving mesh is more sensitive to the choice of slope limiter than is its FV method counterpart. Therefore, future work to improve the performance of the DG scheme even further will likely involve the design of optimal slope limiters. As presently constructed, our technique offers the potential of improved accuracy in astrophysical simulations using the moving mesh AREPO code as well as those employing adaptive mesh refinement (AMR).

Key words: methods: numerical, magnetohydrodynamics

1 INTRODUCTION

Discontinuous Galerkin (DG) methods have recently been implemented for solving systems of conservation laws to arbitrary orders of accuracy, and have been shown to be competitive with more established and traditional finite volume (FV) approaches (Bassi & Rebay 1997a,b; Cockburn, Li & Shu 2004; Luo, Baum & Löhner 2008; Li & Shu 2005). In this paper, we develop a second-order DG formulation for arbitrary moving and static meshes that is appropriate for even the largest astrophysical simulations. DG techniques offer numerous advantages over FV methods, as summarized by Luo, Baum & Löhner (2008). In particular, DG procedures can be applied to arbitrary meshes (moving meshes, adaptive mesh refinement (AMR)) and the method is "compact" in the sense that each cell is treated independently and elements communicate only with adjacent elements having a common face irrespective of the order of accuracy. The DG method is conservative and requires solving the Riemann problem across cell interfaces, similar to FV schemes. The main challenge with DG implementations lies in minimizing unphysical post-shock oscillations (e.g. with slope limiting, flux limiting, shock capturing, or weighted essentially non-oscillatory (WENO) approaches) (Luo, Baum & Löhner 2008), which is also an issue for FV methods. Some DG formulations are found to be more sensitive to certain shock limiters than their FV counterparts, but techniques exist to prevent unphysical oscillatory solutions in high-order DG methods (Hoteit et al. 2004; Ghostine et al. 2009; Luo, Baum & Löhner 2008).

Our DG implementation falls into the class of centroidal Taylor basis procedures developed by Luo, Baum & Löhner (2008). This formulation of DG is relatively new and is quite different from the more widespread approach that employs nodal basis value functions (which would not be generalizable to a moving Voronoi

⋆ E-mail: pmocz@cfa.harvard.edu (PM)
† Hubble Fellow

mesh where the number of faces per cell can change with time). The primary difference between our centroidal DG method and FV schemes is in the manner in which gradients (as well as higher order derivatives) are computed for the solution of fluid variables in a cell. FV methods require the use of an extended stencil (which become spatially broad for estimating higher order terms). DG techniques, on the other hand, evolve the coefficients of a set of basis functions that describe the solution local to a cell in the same way that cell-averages are evolved in the FV approach. This localizes the solution within a given cell, which can lead to reduced numerical errors and makes codes highly parallelizable. The centroidal DG approach may thus be viewed as an extension of the FV method.

Moreover, the DG procedure allows for a locally divergence-free representation of the solution in a cell (Luo, Baum & Löhner 2008; Li & Shu 2005). This not only reduces the amount of memory required to store the result but is also a useful for improving the accuracy of magnetohydrodynamic (MHD) simulations. The continuum equations of ideal MHD impose the condition $\nabla \cdot \mathbf{B} = 0$, but discretized versions of the equations do not necessarily preserve the zero divergence constraint. The locally divergence-free DG method keeps divergences to zero within cell domains unlike FV schemes, but does not guarantee a globally divergence-free solution (equivalent to continuous transverse magnetic field components across cell interfaces) due to the local discontinuous representation of the result (see § 2.6).

The strictest approach for preserving $\nabla \cdot \mathbf{B} = 0$ at the discretized level to machine precision is the Constrained-Transport (CT) framework, developed for the MHD equations by Evans & Hawley (1988). The CT method uses Stoke's theorem to represent the magnetic fields by face-averaged rather than cell-averaged quantities. However, while the CT method can be easily implemented on fixed rectangular grids when a single, fixed timestep is used, it is presently not known whether CT can be adopted for meshes of arbitrary structure, moving meshes, or general time-stepping schemes. The CT approach has been implemented in AMR codes by using synchronized time-stepping and restriction and prolongation operators (Balsara 2001; Fromang, Hennebelle & Teyssier 2006; Miniati & Martin 2011), although this makes the original AMR formulation significantly more complicated. In addition, sometimes CT schemes coupled with Godunov methods need to be modified to prevent pressures from becoming negative at the cost of maintaining conservation of energy to machine precision (Balsara & Spicer 1999). A number of divergence cleaning schemes, such as the Dedner hyperbolic cleaning method and the Powell 8-wave technique, have been developed for controlling global divergence errors in situations where the CT algorithm cannot be employed (Powell et al. 1999; Tóth 2000; Dedner et al. 2002). The locally divergence-free DG implementation, either on its own, or coupled to a cleaning scheme, may improve the divergence-free constraint.

Widely-used grid-based codes for solving fluid flows in astrophysical systems, such as FLASH (Fryxell et al. 2000), ENZO (O'Shea et al. 2004), RAMSES (Fromang, Hennebelle & Teyssier 2006), ATHENA (Stone et al. 2008), and AREPO (Springel 2010) all employ the FV approach. These codes have had numerous successes in simulating cosmological structure formation, galaxy interactions, the interstellar medium, and protoplanetary and accretion discs. Here we investigate whether the DG procedure offers a viable alternative for designing future generations of simulation codes by directly comparing second-order DG and FV methods with the same time integration scheme.

Our goal is to develop a DG algorithm for arbitrary meshes that is efficient and simple in its implementation and, to the extent possible, minimizes numerical errors, artificial diffusion of angular momentum, and global inaccuracies in the magnetic field. We are particularly interested in the application of the method to moving mesh algorithms, such as the AREPO code written by Springel (2010). The moving mesh technique is a novel type of fluid solver that is essentially a hybrid of traditional static Eulerian codes and the pseudo-Lagrangian, mesh-free smoothed particle hydrodynamics (SPH) method. In the moving mesh approach, fluid elements move with the local velocity flow, rendering the method quasi-Lagrangian. This greatly reduces advection errors arising from large bulk velocity motions of the flow, making the code well-suited for simulating galaxy collisions. AREPO has been generalized to solve the Navier-Stokes equations (Muñoz et al. 2013), as well the MHD equations using the Dedner and Powell divergence cleaning schemes (Pakmor, Bauer & Springel 2011; Pakmor & Springel 2012). We show in what follows that the DG scheme can improve the accuracy of the current version of AREPO as well as other FV codes.

Our paper is organized as follows. In § 2 we describe the DG method with centroidal Taylor basis functions and demonstrate how it is a natural generalization of the FV method. In § 3 we present the results of numerical tests in which we compare the DG and FV methods. In § 4 we summarize the main findings of these tests. In § 5 we discuss the advantages of DG methods for astrophysical applications. In § 6 we briefly offer possible ways of refining the slope limiting technique, which could improve the accuracy of the DG method even further. In § 7 we provide conclusions.

2 DISCONTINUOUS GALERKIN FORMULATION

2.1 Governing equations

The ideal MHD equations can be written in conservative form as:

$$\frac{\partial \mathbf{U}}{\partial t} + \nabla \cdot \mathbf{F} = 0, \tag{1}$$

where $\mathbf{U}$ is the conservative state vector and $\mathbf{F}(\mathbf{U})$ is the flux function:

$$\mathbf{U} = \begin{pmatrix} \rho \\ \rho\mathbf{v} \\ \rho e \\ \mathbf{B} \end{pmatrix}, \qquad \mathbf{F} = \begin{pmatrix} \rho\mathbf{v} \\ \rho\mathbf{v}\mathbf{v}^T + p - \mathbf{B}\mathbf{B}^T \\ \rho e\mathbf{v} + p\mathbf{v} - \mathbf{B}(\mathbf{v}\cdot\mathbf{B}) \\ \mathbf{B}\mathbf{v}^T - \mathbf{v}\mathbf{B}^T \end{pmatrix}. \tag{2}$$

Here, ρ is the gas density, $p = p_{\rm gas} + \frac{1}{2}\mathbf{B}^2$ is the total gas pressure, $e = \rho u + \frac{1}{2}\mathbf{v}^2 + \frac{1}{2\rho}\mathbf{B}^2$ is the total energy per unit mass, and u is the thermal energy per unit mass. In the numerical examples described in this paper, we consider an equation of state of the form $p_{\rm gas} = (\gamma - 1)\rho u$, where γ is the adiabatic index.

The above equations reduce to the Euler equations (which describe compressible, inviscid flows) in the case that $\mathbf{B} = 0$.

2.2 Discontinuous Galerkin method

The DG method is defined by first considering the weak formulation of the conservation equations (1) obtained by multiplying by a test function $\mathbf{W}$, integrating over the domain (Ω), and performing an integration by parts:

$$\int_\Omega \frac{\partial \mathbf{U}}{\partial t}\mathbf{W}\, d\Omega + \int_\Gamma \mathbf{F}\cdot\hat{\mathbf{n}}\mathbf{W}\, d\Gamma + \int_\Omega \mathbf{F}\cdot\nabla\mathbf{W}\, d\Omega = 0, \tag{3}$$

where $\Gamma = \partial\Omega$ is the boundary of Ω and $\hat{\mathbf{n}}$ is the outward unit normal vector of the boundary.

We seek to discretize Equation (3). We begin by writing the solution in each cell e as a second-order accurate Taylor series expansion about the centroid (x_c, y_c), and employing coordinates (x, y) with origin at (x_c, y_c). For example, in 2D:

$$\mathbf{U}_e = \tilde{\mathbf{U}}_e + \frac{\partial \mathbf{U}_e}{\partial x}|_c x + \frac{\partial \mathbf{U}_e}{\partial y}|_c y, \tag{4}$$

where $\tilde{\mathbf{U}}_e$ is the cell average of the fluid variables. Our local basis functions for each fluid variable are:

$$V_1 = 1,\, V_2 = x,\, V_3 = y, \tag{5}$$

and the unknowns in this problem are the cell averages and the cell derivatives.

If we use the basis functions V_i each as possible test functions $\mathbf{W}$, we obtain a set of evolution equations for the cell averages and derivatives (see also Luo, Baum & Löhner (2008) for a formal mathematical presentation of centroidal DG methods):

$$\frac{d}{dt}\int_{\Omega_e} \tilde{\mathbf{U}}_e \, d\Omega + \int_{\Gamma_e} \mathbf{F}(\mathbf{U}_e)\cdot\hat{\mathbf{n}}\, d\Gamma = 0, \tag{6}$$

$$\begin{aligned}\frac{d}{dt}\int_{\Omega_e} \begin{pmatrix} x^2 & xy \\ xy & y^2 \end{pmatrix} \begin{pmatrix} \frac{\partial U_{e,i}}{\partial x}|_c \\ \frac{\partial U_{e,i}}{\partial y}|_c \end{pmatrix} d\Omega \\ + \int_{\Gamma_e} \mathbf{F}(U_{e,i})\cdot\hat{\mathbf{n}} \begin{pmatrix} x \\ y \end{pmatrix} d\Gamma \\ - \int_{\Omega_e} \mathbf{F}(U_{e,i})\cdot\nabla \begin{pmatrix} x \\ y \end{pmatrix} d\Omega \\ = 0,\end{aligned} \tag{7}$$

where $U_{e,i}$ is a single component of $\mathbf{U}_e$. Thus, the x and y derivatives are coupled and it is necessary to invert a 2 by 2 matrix to obtain the derivatives.

We see from Equations (6) and (7) that the cell-averages and cell derivatives decouple for the choice of the Taylor-basis function. In fact, Equation (6) is the same equation used to update a FV scheme. Thus the centroidal DG method is a natural higher order generalization of the FV approach if one asserts that cells are only allowed to communicate with their nearest neighbors.

The matrix

$$M = \int_{\Gamma_e} \begin{pmatrix} x^2 & xy \\ xy & y^2 \end{pmatrix} d\Omega \tag{8}$$

in Equation (7) is called the mass matrix. It stores second-order moments of the cell (which have to be computed for every active cell at every timestep in a moving mesh approach, and every time a cell is refined in an AMR approach) and is symmetric. The moments for each cell are calculated exactly using Gaussian quadrature.

In the 3D case, using a Taylor basis we have the following weak formulation of the Euler equations for a cell e (again, coordinates (x, y, z) in the notation below have origin (x_c, y_c, z_c)):

$$\frac{d}{dt}\int_{\Omega_e} \tilde{\mathbf{U}}_e \, d\Omega + \int_{\Gamma_e} \mathbf{F}(\mathbf{U}_e)\cdot\hat{\mathbf{n}}\, d\Gamma = 0, \tag{9}$$

$$\begin{aligned}\frac{d}{dt}\int_{\Omega_e} \begin{pmatrix} x^2 & xy & xz \\ xy & y^2 & yz \\ xz & yz & z^2 \end{pmatrix} \begin{pmatrix} \frac{\partial U_{e,i}}{\partial x}|_c \\ \frac{\partial U_{e,i}}{\partial y}|_c \\ \frac{\partial U_{e,i}}{\partial z}|_c \end{pmatrix} d\Omega \\ + \int_{\Gamma_e} \begin{pmatrix} \mathbf{F}(U_{e,i})\cdot\hat{\mathbf{n}}\, x \\ \mathbf{F}(U_{e,i})\cdot\hat{\mathbf{n}}\, y \\ \mathbf{F}(U_{e,i})\cdot\hat{\mathbf{n}}\, z \end{pmatrix} d\Gamma \\ - \int_{\Omega_e} \begin{pmatrix} \mathbf{F}_x(U_{e,i}) \\ \mathbf{F}_y(U_{e,i}) \\ \mathbf{F}_z(U_{e,i}) \end{pmatrix} d\Omega \\ = 0.\end{aligned} \tag{10}$$

Now if we define the volume and moment-averaged quantities $\mathbf{Q}_e$ and $\mathbf{R}_e$ as:

$$\mathbf{Q}_e = \int_{\Omega_e} \mathbf{U}_e \, d\Omega, \tag{11}$$

$$\mathbf{R}_{e,i} = \int_{\Omega_e} \begin{pmatrix} x^2 & xy & xz \\ xy & y^2 & yz \\ xz & yz & z^2 \end{pmatrix} \begin{pmatrix} \frac{\partial U_{e,i}}{\partial x}|_c \\ \frac{\partial U_{e,i}}{\partial y}|_c \\ \frac{\partial U_{e,i}}{\partial z}|_c \end{pmatrix} d\Omega \tag{12}$$

then we can write a second-order conservative discretization in time of Equations (9) and (10):

$$\mathbf{Q}_e^{(n+1)} = \mathbf{Q}_e^{(n)} - \Delta t \sum_f A_{ef} \hat{\mathbf{F}}_{ef}^{(n+1/2)}, \tag{13}$$

$$\begin{aligned}\mathbf{R}_{e,i}^{(n+1)} = \mathbf{R}_{e,i}^{(n)} \\ - \Delta t \sum_f A_{ef} \hat{\mathbf{F}}_{ef}(U_{e,i})^{(n+1/2)} \begin{pmatrix} c_{ef,x} \\ c_{ef,y} \\ c_{ef,z} \end{pmatrix} \\ + \Delta t \int_{\Omega_e} \begin{pmatrix} \mathbf{F}_x(U_{e,i})^{(n+1/2)} \\ \mathbf{F}_y(U_{e,i})^{(n+1/2)} \\ \mathbf{F}_z(U_{e,i})^{(n+1/2)} \end{pmatrix} d\Omega,\end{aligned} \tag{14}$$

where $\hat{\mathbf{F}}_{ef}^{(n+1/2)}$ is an appropriately time-averaged approximation to the true flux $\mathbf{F}_{ef}$ across a cell face between cells e and f, A_{ef} is the area of the cell face, and $(c_{ef,x}, c_{ef,y}, c_{ef,z})$ is the location of the centroid of the cell face in the coordinate system local to cell e. The volume integral in the interior of the cell is carried out with Gaussian quadrature.

The basic idea of the DG method is to update $\mathbf{Q}_e$ and $\mathbf{R}_e$ for each active cell during each timestep. One can then obtain the cell averages of conserved fluid variables at the end of the step by dividing the $\mathbf{Q}_e$ by the cell volume (and consequently translated to primitive variables). Derivative information is obtained by matrix inversion of the mass matrix applied to $\mathbf{R}_e$. Derivatives of primitive variables may then be calculated by expanding the derivatives and solving for the primitive gradients, as, for example:

$$\begin{aligned}\frac{\partial(\rho v_x)}{\partial y} = \rho\frac{\partial(v_x)}{\partial y} + v_x\frac{\partial(\rho)}{\partial y} \\ \Rightarrow \frac{\partial(v_x)}{\partial y} = \frac{1}{\rho}\left(\frac{\partial(\rho v_x)}{\partial y} - v_x\frac{\partial(\rho)}{\partial y}\right).\end{aligned} \tag{15}$$

Finally, in order to represent magnetic fields, we use a locally

divergence-free basis (e.g. in 2D) for $\begin{pmatrix} B_x \\ B_y \end{pmatrix}$ instead of a Taylor basis, in particular:

$$\mathbf{V}_1 = \begin{pmatrix} 1 \\ 0 \end{pmatrix}, \mathbf{V}_2 = \begin{pmatrix} 0 \\ 1 \end{pmatrix}, \mathbf{V}_3 = \begin{pmatrix} y \\ 0 \end{pmatrix}, \mathbf{V}_4 = \begin{pmatrix} 0 \\ x \end{pmatrix}, \mathbf{V}_5 = \begin{pmatrix} x \\ -y \end{pmatrix}. \tag{16}$$

The number of required basis functions is reduced from 6 to 5 owing to the divergence-free constraint. We derive an equation for the evolution of the magnetic field gradients analogously to Equation (7); namely:

$$\begin{aligned} &\frac{d}{dt}\int_{\Omega_e} \begin{pmatrix} y^2 & 0 & xy \\ 0 & x^2 & -xy \\ xy & -xy & x^2+y^2 \end{pmatrix} \begin{pmatrix} \alpha_1 \\ \alpha_2 \\ \alpha_3 \end{pmatrix} \\ &+ \int_{\Gamma_e} \begin{pmatrix} \mathbf{F}(B_x)\cdot\hat{\mathbf{n}}\, y \\ \mathbf{F}(B_y)\cdot\hat{\mathbf{n}}\, x \\ \mathbf{F}(B_x)\cdot\hat{\mathbf{n}}\, x - \mathbf{F}(B_y)\cdot\hat{\mathbf{n}}\, y \end{pmatrix} d\Gamma \\ &- \int_{\Omega_e} \begin{pmatrix} \mathbf{F}_y(B_x) \\ \mathbf{F}_x(B_y) \\ \mathbf{F}_x(B_x) - \mathbf{F}_y(B_y) \end{pmatrix} d\Omega \\ &= 0, \end{aligned} \tag{17}$$

where

$$\alpha_1 = \frac{\partial B_x}{\partial y}, \tag{18}$$

$$\alpha_2 = \frac{\partial B_y}{\partial x}, \tag{19}$$

$$\alpha_3 = \frac{\partial B_x}{\partial x} = -\frac{\partial B_x}{\partial x}, \tag{20}$$

and the coordinates (x, y) have origin (x_c, y_c). In this case, a 3 by 3 matrix has to be inverted to directly obtain all the magnetic field gradients.

In 3D, locally divergence-free basis functions may be chosen as:

$$\begin{aligned} \mathbf{V}_1 = \begin{pmatrix} 1 \\ 0 \\ 0 \end{pmatrix}, \mathbf{V}_2 = \begin{pmatrix} 0 \\ 1 \\ 0 \end{pmatrix}, \mathbf{V}_3 = \begin{pmatrix} 0 \\ 0 \\ 1 \end{pmatrix}, \\ \mathbf{V}_4 = \begin{pmatrix} y \\ 0 \\ 0 \end{pmatrix}, \mathbf{V}_5 = \begin{pmatrix} z \\ 0 \\ 0 \end{pmatrix}, \\ \mathbf{V}_6 = \begin{pmatrix} 0 \\ x \\ 0 \end{pmatrix}, \mathbf{V}_7 = \begin{pmatrix} 0 \\ z \\ 0 \end{pmatrix}, \\ \mathbf{V}_8 = \begin{pmatrix} 0 \\ 0 \\ x \end{pmatrix}, \mathbf{V}_9 = \begin{pmatrix} 0 \\ 0 \\ y \end{pmatrix}, \\ \mathbf{V}_{10} = \begin{pmatrix} x \\ -y \\ 0 \end{pmatrix}, \mathbf{V}_{11} = \begin{pmatrix} x \\ 0 \\ -z \end{pmatrix}. \end{aligned} \tag{21}$$

In which case one obtains the weak formulation of the evolution equation for the coefficients of the bases that determine the derivatives ($\alpha_3, \ldots, \alpha_{11}$):

$$\begin{aligned} &\frac{d}{dt}\int_{\Omega_e} \mathbf{M}_B \begin{pmatrix} \alpha_3 \\ \alpha_4 \\ \alpha_5 \\ \alpha_6 \\ \alpha_7 \\ \alpha_8 \\ \alpha_9 \\ \alpha_{10} \\ \alpha_{11} \end{pmatrix} \\ &+ \int_{\Gamma_e} \begin{pmatrix} \mathbf{F}(B_x)\cdot\hat{\mathbf{n}}\, y \\ \mathbf{F}(B_x)\cdot\hat{\mathbf{n}}\, z \\ \mathbf{F}(B_y)\cdot\hat{\mathbf{n}}\, x \\ \mathbf{F}(B_y)\cdot\hat{\mathbf{n}}\, z \\ \mathbf{F}(B_z)\cdot\hat{\mathbf{n}}\, x \\ \mathbf{F}(B_z)\cdot\hat{\mathbf{n}}\, y \\ \mathbf{F}(B_x)\cdot\hat{\mathbf{n}}\, x - \mathbf{F}(B_y)\cdot\hat{\mathbf{n}}\, y \\ \mathbf{F}(B_x)\cdot\hat{\mathbf{n}}\, x - \mathbf{F}(B_z)\cdot\hat{\mathbf{n}}\, z \end{pmatrix} d\Gamma \\ &- \int_{\Omega_e} \begin{pmatrix} \mathbf{F}_y(B_x) \\ \mathbf{F}_z(B_x) \\ \mathbf{F}_x(B_y) \\ \mathbf{F}_z(B_y) \\ \mathbf{F}_x(B_z) \\ \mathbf{F}_y(B_z) \\ \mathbf{F}_x(B_x) - \mathbf{F}_y(B_y) \\ \mathbf{F}_x(B_x) - \mathbf{F}_z(B_z) \end{pmatrix} d\Omega \\ &= 0, \end{aligned} \tag{22}$$

where

$$\mathbf{M}_B = \begin{pmatrix} y^2 & yz & 0 & 0 & 0 & 0 & xy & xy \\ yz & z^2 & 0 & 0 & 0 & 0 & xz & xz \\ 0 & 0 & x^2 & xz & 0 & 0 & -xy & 0 \\ 0 & 0 & xz & x^2 & 0 & 0 & -zy & 0 \\ 0 & 0 & 0 & 0 & x^2 & xy & 0 & -xz \\ 0 & 0 & 0 & 0 & xy & y^2 & 0 & -yz \\ xy & xz & -xy & -xz & 0 & 0 & x^2-y^2 & x^2 \\ xy & xz & 0 & 0 & -xz & -yz & x^2 & x^2-z^2 \end{pmatrix}. \tag{23}$$

2.3 Fluid dynamics on a moving mesh

In the case of non-static meshes, the Euler and MHD equations need to be modified to account for the motion of the grid. The flux over an interface moving at velocity $\mathbf{w}$ or inside a cell moving at velocity $\mathbf{w}$ is a combination of the static flux and an advection step due to the movement:

$$\mathbf{F}_{\mathrm{m}}(\mathbf{U}) = \mathbf{F}_{\mathrm{s}}(\mathbf{U}) - \mathbf{U}\mathbf{w}^T. \tag{24}$$

All Riemann problems across cell interfaces are solved in the rest-frame of the face, followed by adding appropriate terms to return to the lab frame, as described in detail in Pakmor, Bauer & Springel (2011) (see their equation 17). This approach retains a stable, upwind character. The Riemann problem is solved using an exact solver for the Euler equations and an HLLD solver (Miyoshi & Kusano 2005) for the MHD equations.

2.4 Time stepping

We use a second-order accurate in time MUSCL-Hancock scheme to update the fluid variables at the next timestep, the same method

as is used for AREPO's FV solver, described in Springel (2010). In the MUSCL-Hancock procedure (van Leer 1974; Toro 1999) the essential idea is to use cell averages to predict the values of the primitive quantities at cell edges half a timestep in advance (equation (18) of Springel (2010)), and use these predicted values to solve the Riemann problem and obtain $\hat{\mathbf{F}}_{ef}^{(n+1/2)}$ in order to finish updating the solution to the next timestep. The same prediction equations are also used to calculate the flux in the interior of the cell in the volume integral term of Equation (14). We find that this explicit time-updating scheme works very well for our DG method. Our approach is different from traditional DG formulations that typically use explicit or implicit Runge-Kutta techniques (Luo, Baum & Löhner 2008). A benefit of using the second-order MUSCL-Hancock integrator is that it can be coupled with a symplectic second-order gravity solver to treat fluids with self-gravity (Springel 2010).

The fact that we use the same time integration scheme for the DG and FV methods allow us to compare the advantages of one over the other in a direct manner. The primary difference in the second-order DG technique compared to the FV approach is only in the way in which cell gradients are handled. In a timestep, it is the quantity

$$\int \mathbf{R}_{e,i} = M \begin{pmatrix} \frac{\partial U_{e,i}}{\partial x}|_c \\ \\ \frac{\partial U_{e,i}}{\partial y}|_c \end{pmatrix} d\Omega \tag{25}$$

that is evolved by Equation (14) in a quite similar manner as volume averaged conserved quantities are evolved in a FV scheme. After each timestep update, the matrix system of equations is then inverted to obtain the gradients of the conserved variables, which are then transformed to gradients of the primitive variables (just as cell volume integrated conserved variables are converted to cell-averaged primitive variables) for the next half-timestep prediction step in the MUSCL-Hancock scheme.

2.5 Slope limiter

For the static and moving FV method and the static DG method, we use the original slope limiter in AREPO (Springel 2010). This limiter requires that the linearly reconstructed quantities on face centroids do not exceed the maxima or minima among all neighbouring cells. Each gradient is replaced with a slope-limited gradient:

$$\langle \nabla \phi \rangle_i' = \alpha_i \langle \nabla \phi \rangle_i, \tag{26}$$

where the slope limiter coefficient $0 \leq \alpha_i \leq 1$ is computed as:

$$\alpha_i = \min(1, \psi_{ij}) \tag{27}$$

$$\psi_{ij} = \begin{cases} (\phi_i^{\max} - \phi_i)/\Delta\phi_{ij} & \text{for } \Delta\phi_{ij} > 0 \\ (\phi_i^{\min} - \phi_i)/\Delta\phi_{ij} & \text{for } \Delta\phi_{ij} < 0 \\ 1 & \text{for } \Delta\phi_{ij} = 0 \end{cases}. \tag{28}$$

Here, $\Delta\phi_{ij} = \langle \nabla\phi \rangle_i \cdot (\mathbf{f}_{ij} - \mathbf{s}_i)$ is the estimated change between the centroid $\mathbf{f}_{ij}$ of the face and the centre of cell i, and $\phi_i^{\max} = \max(\phi_j)$ and $\phi_i^{\min} = \min(\phi_j)$ are the maximum and minimum values occurring for ϕ among all neighbouring cells of cell i, including i itself.

We find that the DG method on a moving mesh is quite sensitive to the choice of slope limiter and the above form results in excessive post-shock oscillations in certain test problems, likely due to the fact that it is not total variation diminishing (TVD) and that it also limits local smooth extrema. Identifying a robust limiter which is not too dissipative is still an open problem for the moving DG method. In what follows, we adopt a limiter which is similar in spirit to a WENO method (Luo, Baum & Löhner 2007). We find this limiter to be robust for all of our tests and use it as the best, *default choice* for all test problems.

For each cell i we consider two candidate values for the slope of a primitive fluid variable ϕ. One candidate is the slope-limited gradient obtained with a stencil, as in the FV method (in the case of the magnetic field gradient we project it to a divergence-free space). The other candidate is the unlimited DG local gradient. For each candidate k we compute an oscillation factor:

$$o_{ik} = \sum_j |\Delta\phi_{ij}| + |\phi_j - (\phi_i + \Delta\phi_{ij})|. \tag{29}$$

The slope is then a weighted sum of the candidates:

$$\langle \nabla\phi \rangle_i' = \frac{\sum_k \langle \nabla\phi \rangle_{ik} \cdot \frac{1}{(\epsilon + o_{ik})^\gamma}}{\sum_k \frac{1}{(\epsilon + o_{ik})^\gamma}}, \tag{30}$$

where ϵ is machine epsilon and $\gamma = 0.5$. The slope-limiting occurs at the beginning of each timestep, before any prediction steps or updating take place. Following the limiting step, the quantities in Equation (25) are also re-calculated.

In all of our numerical tests, we use the slope limiter of Springel (2010) for the static and moving FV results and the static DG results. However, we use the modified WENO-type limiter as the default choice for the moving DG results because we find it is much more robust and reduces non-physical oscillations to a minimum. In a couple of our numerical tests with the moving DG method, we present the results of the original limiting scheme (labelled as 'limiter 2') for comparison, although we favour the alternate limiter for the moving DG method.

2.6 Magnetic field divergence errors

When solving the Riemann problem across flux interfaces, a constant magnetic field perpendicular to the interface must be assumed. We use the average value of the perpendicular magnetic fields extrapolated from the left and right sides of the interface: $B_x = \frac{1}{2}(B_{x,L} + B_{x,R})$. This means that despite having a locally divergence-free representation of the magnetic field inside each cell in the DG formulation, there is still a divergence error estimated by Stokes theorem:

$$\nabla \cdot \mathbf{B}_i = \frac{1}{\mathcal{V}_i} \sum_{\text{faces}} \mathbf{B} \cdot \hat{\mathbf{n}} A_i, \tag{31}$$

where $\mathcal{V}_i$ is the volume of cell i, and we sum (over the faces) the outward normal values of the magnetic field multiplied by the area of the face. However, a locally divergence free representation of the magnetic field is expected to reduce global divergence errors because the contribution to the divergence error from within each cell is exactly zero.

3 RESULTS OF NUMERICAL TESTS

We perform a series of numerical tests documented in the literature to compare the static and moving DG and FV methods. The results of these tests are presented in the following subsections.

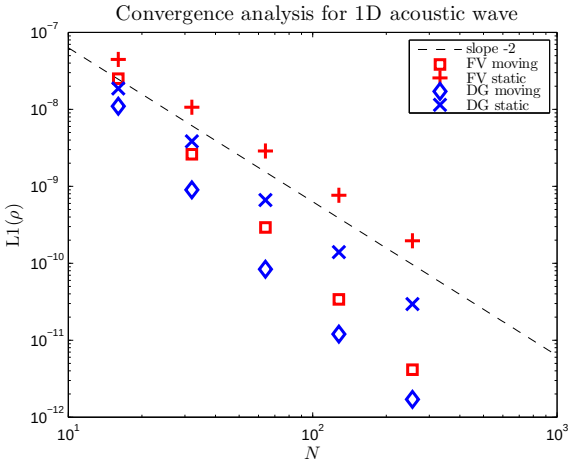

Figure 1. Convergence of the 1D acoustic wave in the L1 norm. Second-order convergence is achieved, as expected (in fact the moving mesh schemes show superconvergence). The DG and FV methods are compared on static and moving meshes. The moving DG technique produces the smallest errors. Errors are ~ 60 per cent smaller than the moving FV approach. The static DG method has errors ~ 80 smaller than the static FV scheme.

3.1 1D acoustic wave

The first test we present is a simple 1D acoustic wave, discussed in Stone et al. (2008), and also described in Springel (2010). This setup serves as a sensitive test of the convergence rate of a code. A simple acoustic wave of unit wavelength is initialized with very small amplitude $\Delta\rho/\rho = 10^{-6}$ and $\rho = 1$ in a periodic domain of unit length. The gas has pressure $p = 3/5$ and adiabatic index $\gamma = 5/3$. The L1 error norm is computed when the wave returns to its original position (the analytic solution here is identical to the initial state). Fig. 1 shows the L1 error norms for the moving and static DG and FV methods as a function of mesh resolution. Second-order convergence is achieved, as expected. The moving and static DG algorithms show a ~ 60 per cent and ~ 80 per cent reduction of errors over their FV counterparts, respectively.

3.2 1D Sod shock tube

We continue our investigation by simulating a 1D Sod shock tube. We adopt initial conditions employed in a large number of other code tests (Hernquist & Katz 1989; Rasio & Shapiro 1991; Wadsley, Stadel & Quinn 2004; Springel 2005, 2010). The left side ($x < 0$) is described by $p_L = 1$, $\rho_L = 1$, $v_L = 0$, the right side ($x \geq 0$) is described by $p_R = 0.1795$, $\rho_R = 0.25$, $v_R = 0$, and the gas as adiabatic index $\gamma = 1.4$. We evolve the system until $t = 5.0$. The solutions in the moving FV and DG formulations are shown in Fig. 2.

The DG method does a superior job of maintaining sharp shock interfaces while at the same time reducing post-shock oscillations (especially in velocity). Typically one might expect a trade-off between sharpness and reduction of non-physical oscillations. We note that the DG method on a moving mesh uses the modified WENO-type slope limiter (the limiter of Springel (2010) produces overly severe non-physical oscillations). In both the moving FV and moving DG schemes, the shock discontinuities are typically broadened over two cells, but the slopes in the DG version are larger. On static grids (not shown) the shock discontinuities typically span three cells at this resolution and time in the simulation. Error convergence plots for moving and static approaches are shown in Fig. 3, where it is seen that DG methods again have advantages over their FV counterparts. The method is first-order accurate in this test problem because the solution has to be slope-limited owing to the presence of the shock discontinuity.

We also consider a strong shock version of the shock tube (Mach number $M = 6.3$), as studied in Sijacki et al. (2012). The initial conditions are $P_L = 30.0$, $\rho_L = 1.0$, $v_L = 0$, $P_R = 0.14$, $\rho_R = 0.125$, $v_R = 0$, $\gamma = 1.4$. Moving mesh codes (as opposed to static mesh codes) may exhibit a 'spike' in the entropy at the contact discontinuity (which can be eliminated with smoothed initial conditions). The feature is due to the fact that moving mesh codes preserve contact discontinuities, present in the initial conditions, to much higher precision than do static mesh codes. In Fig.. 4 we present the entropy profile for the strong shock at t = 5.0, which shows that the DG method also exhibits a 'spike' feature, albeit of somewhat reduced magnitude and has smaller post-shock oscillations after the contact discontinuity. We note again that the DG method on a moving mesh uses the modified WENO-type slope limiter.

3.3 Gresho vortex

We move on to a 2D test for the conservation of vorticity and angular momentum. The problem proposed by Gresho & Chan (1990) considers a static 'triangle vortex'. We adopt the initial conditions described in Liska & Wendroff (2003). The vortex has azimuthal velocity profile:

$$v_\phi(r) = \begin{cases} 5r & \text{for } 0 \leq r < 0.2 \\ 2 - 5r & \text{for } 0.2 \leq r < 0.4 \\ 0 & \text{for } r \geq 0.4 \end{cases}. \quad (32)$$

The gas has constant density $\rho = 1$ and adiabatic index $\gamma = 5/3$. The pressure profile:

$$p(r) = \begin{cases} 5 + \frac{25}{2}r^2 & \text{for } 0 \leq r < 0.2 \\ 9 + \frac{25}{2}r^2 - 20r + 4\ln(r/0.2) & \text{for } 0.2 \leq r < 0.4 \\ 3 + 4\ln 2 & \text{for } r \geq 0.4 \end{cases} \quad (33)$$

balances the centrifugal force with the pressure gradient so that the vortex is a steady-state solution.

Developing a scheme that minimizes angular momentum diffusion for grid-based methods is important because lack of angular momentum conservation is one of the main disadvantages of grid-based methods relative to SPH, which conserves total angular momentum due to its pseudo-Lagrangian character (Price 2012). (We note, however, that this "advantage" of SPH comes at the expense of an inaccurate handling of the mass continuity equation, as discussed by Vogelsberger et al. (2012).) The solutions of the Gresho vortex problem are shown in Fig. 5 and an error convergence plot is presented in Fig. 6. The static DG approach performs significantly better than the static FV method, likely owing to the purely local manner in which it handles gradients, and the moving DG approach offers a small improvement over the moving FV method here. In this test, the static DG method shows an advantage over the moving DG scheme, attributable to the differences in their slope limiters. We used the same slope limiter for the static DG, static FV, and moving FV methods, while for the moving DG approach we find it is generally better to take a weighted average of the local

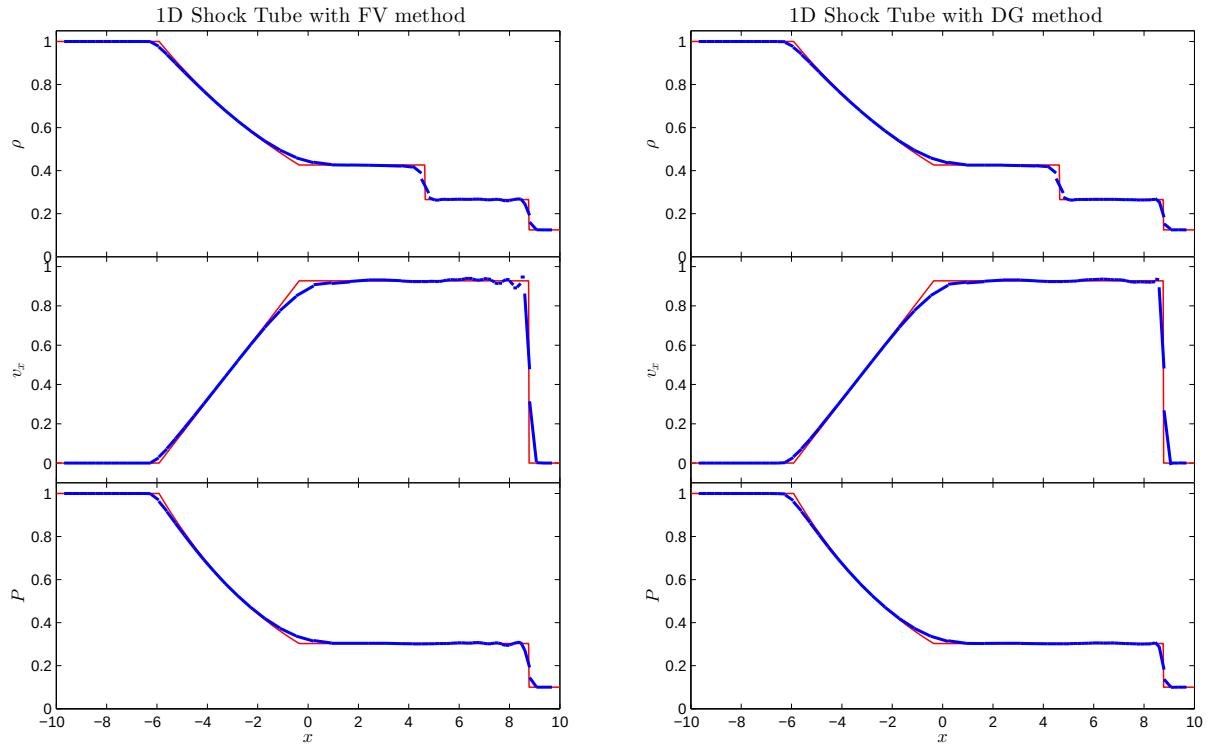

Figure 2. Solution of the 1D shock tube test at $t = 5.0$ (resolution 64) with the moving FV method (left) and the moving DG method (right). The moving DG method reduces post-shock oscillations noticeably (especially in the velocity) while also being less diffusive.

slope of a cell and the one obtained with a stencil to prevent spurious oscillations. This weighting step prevents the gradient from being treated purely locally, since we use a stencil-estimated slope in the stencil. Further refinement of the slope limiter could lead to improvements in the moving DG scheme to the level of the static DG method in this test.

We also verified with additional tests that the static DG approach maintains its strong advantage over the static FV approach on arbitrary meshes. The regularity of a Cartesian grid is not a necessary requirement for the DG method to work well.

3.4 2D implosion

Next we perform a 2D implosion test (Hui, Li & Li 1999) with periodic boundary conditions, as in Sijacki et al. (2012). The domain is a box of side length 0.3. The initial pressure and density are $p = 1.0$, $\rho = 1.0$ for $x + y > 0.15$ and $p = 0.14$, $\rho = 0.125$ otherwise. The gas is initially at rest and has adiabatic index $\gamma = 1.4$. This test is well suited for studying interacting shocks, Richtmyer-Meshkov instabilities, diffusivity, and ability of codes to maintain a symmetric solution.

The development of the implosion is presented in Fig. 7 at several resolutions. We see that the DG method produces less diffusive results than the FV method. In this particular example, the original limiter adopted by Springel (2010) works well for the moving DG method (labelled as 'limiter 2' in the figure), producing sharp shock interfaces, and so we show the results of both limiters for the moving DG method. A point of interest to examine is the low-density region that develops in the bottom left corner of the simulations. The further along diagonally (towards the center) the structure has developed, the less numerical diffusion is present. In

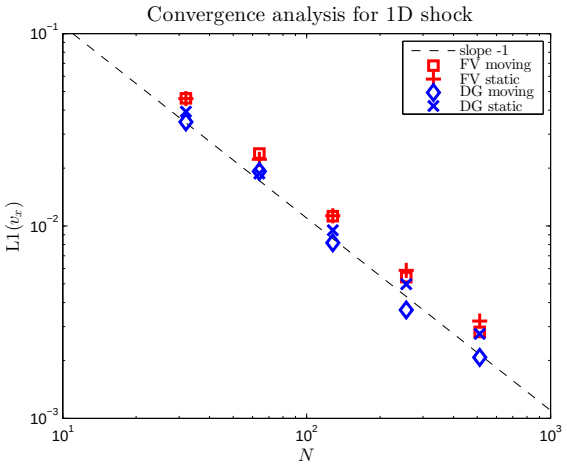

Figure 3. Convergence of the 1D shock tube test in the L1 norm. First-order convergence is achieved, as expected due to the discontinuity in the solution. The DG method on a moving mesh produces the smallest errors, a ~ 30 per cent reduction over the moving FV method.

the cases of static DG and moving DG with limiter 2, the region obtained at a resolution of 128^2 resembles more closely the solution obtained by the FV approach at twice the resolution 256^2 rather than at the same resolution 128^2. This suggests that a purely local treatment of derivatives (no stencils) as in the DG method allows for a better treatment of fluid instabilities and increases the effective resolution of the simulation. The moving FV and moving DG results with the WENO-type limiter are fairly similar, but the DG solution shows that the low-density feature has advanced fur-

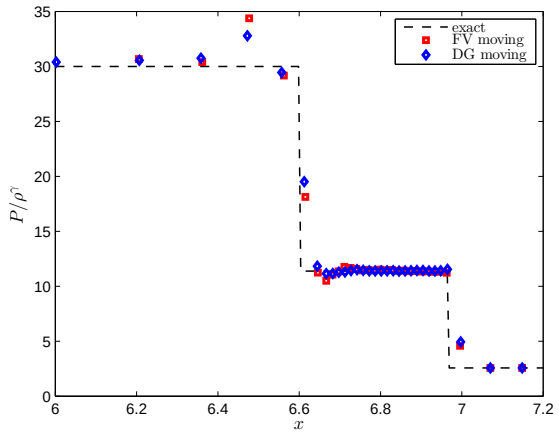

Figure 4. Entropy profile of a strong shock ($M = 6.3$) at $t = 5.0$.

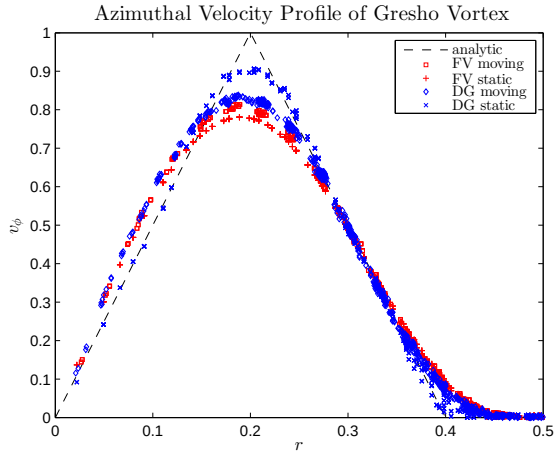

Figure 5. Solution to the 2D Gresho vortex problem at $t = 3.0$, at resolution 32^2. DG methods exhibit reduced levels of angular momentum diffusion owing to treating the gradient of a cell in a completely local manner. Here the static DG method shows an advantage over the moving DG method due to the differences in their slope limiters. Static DG, static FV, and moving FV all have the same slope limiter, while for the moving DG method we find it is generally better to take a weighted average of the local slope of a cell and the one obtained with a stencil to prevent spurious oscillations.

ther diagonally, indicating less numerical diffusion. Note that there are some asymmetries that develop in the moving mesh approach owing to the fact that in our implementation the fluxes across interfaces are added in an arbitrary order and slight differences can arise from finite-precision arithmetic which can be amplified by the additional degree of freedom of the motion of the mesh (we call this effect 'mesh noise'). The appearance and the magnitude of these asymmetries are sensitive to the mesh regularization options, and one could obtain more symmetric results with careful fine-tuning of the regularization parameters.

3.5 Kelvin-Helmholtz instability

In the next test we consider shear flow in 2D which produces Kelvin Helmholtz (KH) instabilities. The initial conditions are those of Springel (2010). In a periodic box of side length 1.0 gas is set up

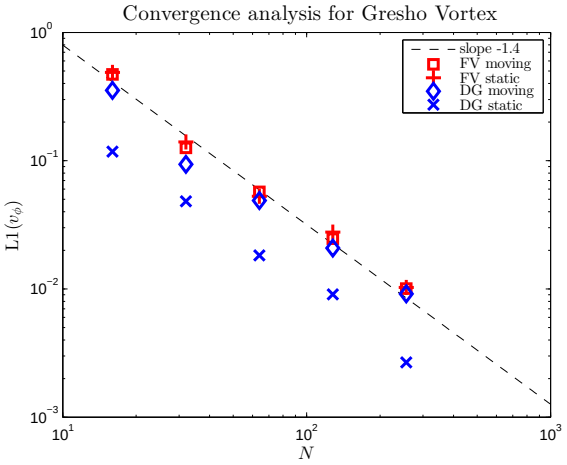

Figure 6. Convergence of the 2D Gresho vortex test in the L1 norm. We display the error in v_ϕ, which is a measure of angular momentum diffusion. Here the static DG method shows a $\sim$ 70 per cent improvement over the other methods.

to have uniform pressure $p = 2.5$ and adiabatic index $\gamma = 5.3$. The density is stratified vertically and has value $\rho = 2$ in the central (red) region, and $\rho = 1$ in the regions at the top and bottom of the box (blue), as indicated in Fig. 8. As mixing occurs, the other colours denote the corresponding intermediate fluid densities. The velocity in the central horizontal strip $|y - 0.5| < 0.25$ has value $v_x = 0.5$ to the right, while the rest of the box has the fluid moving to the left at $v_x = -0.5$. In addition we add a perturbation:

$$v_y(x, y) = w_0 \sin(4\pi x) \times \left(\exp\left[-\frac{-(y-0.25)^2}{2\sigma^2} \right] + \exp\left[-\frac{-(y-0.75)^2}{2\sigma^2} \right] \right) \quad (34)$$

with $w_0 = 0.1$ and $\sigma = 0.5/\sqrt{2}$ in order to excite a single mode of the instability with wavelength equal to half the box size. The results of the various solvers are shown in Fig. 8. The static DG method is better than the static FV method at resolving secondary KH instabilities that develop over the primary KH-billows, which the moving mesh approaches resolve. The moving FV and moving DG methods develop qualitatively similar structures, with small scale structures being well-preserved rather than mixed. The DG method that uses the original limiter ('limiter 2') resolves small features but also exhibits more diffusive mixing.

3.6 3D subsonic driven turbulence

For a 3D test, we consider isothermal gas in a periodic box being turbulently driven by external stochastic forcing on large scales, as examined by Bauer & Springel (2012). We use the driving routine and parameters for Mach number $M = 0.3$ turbulence listed in Table 4 of Bauer & Springel (2012). We are interested in how well the static and moving DG methods can reproduce a Kolmogorov-like velocity power spectrum ($P(k) \propto k^{-5/3}$). In Fig. 9 we present plots of the velocity magnitudes with our various methods at $t = 25.6$, computed at a resolution of 128^3. In Fig. 10 the accompanying velocity power spectra are presented. The results agree with the expectations for a Kolmogorov cascade on the largest spatial scales. The DG method does an improved job of resolving the power to smaller spatial scales with the same number of cells. The

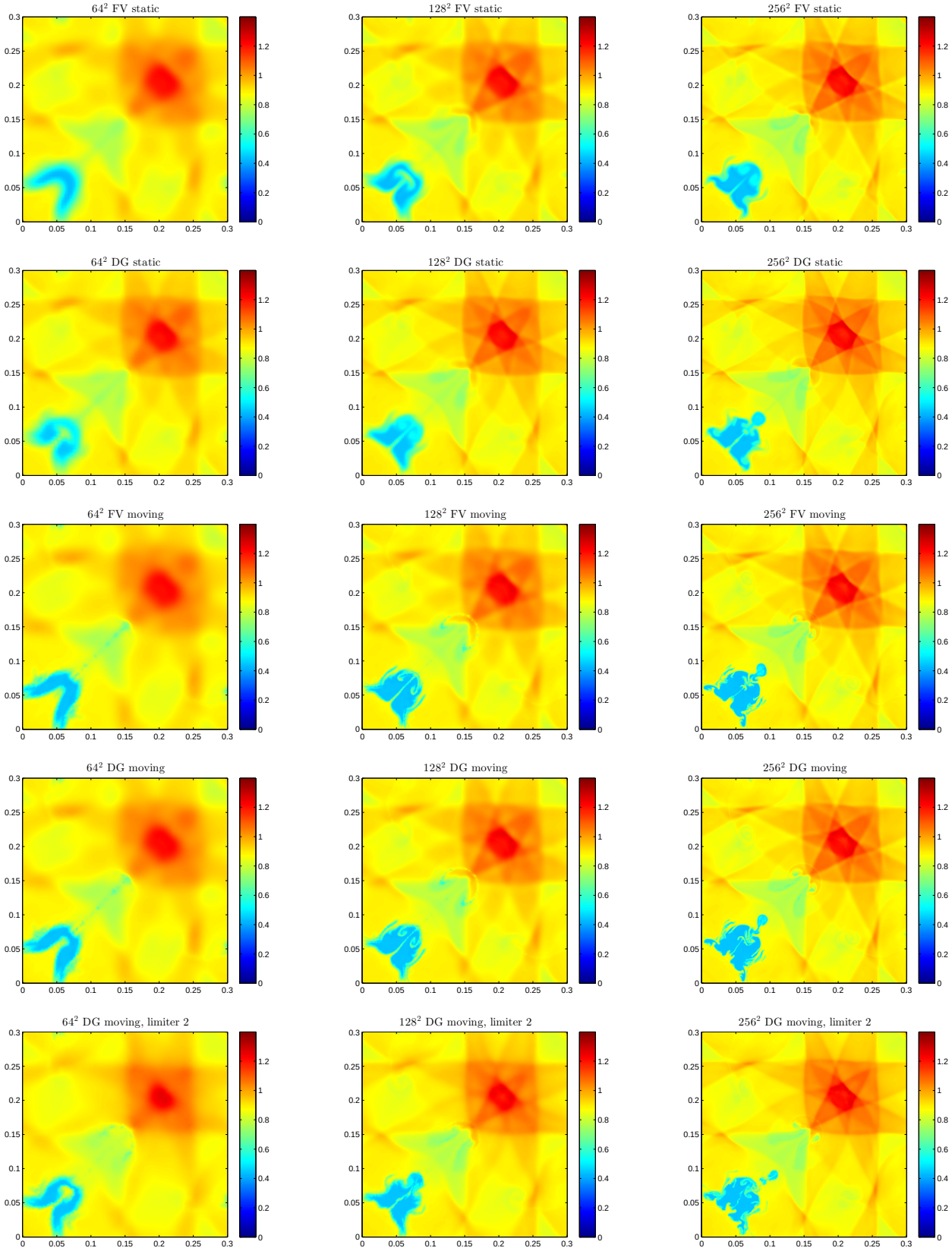

Figure 7. Implosion test ($t = 1.0$, periodic boundary conditions) plots of density for moving and static FV and DG methods at resolutions of 64^2, 128^2, and 256^2. We have also included results of the moving DG method with the same limiter as static FV, moving FV and static DG (limiter 2), which shows the best results in this test, although in general we prefer the modified limiter. The presence of asymmetry in the moving mesh simulations is due to mesh noise. The static DG method and the moving DG method (limiter 2) resolve features of the instability that occur in the low density region in the lower left-hand corner which their FV counterparts resolve only at twice the resolution.

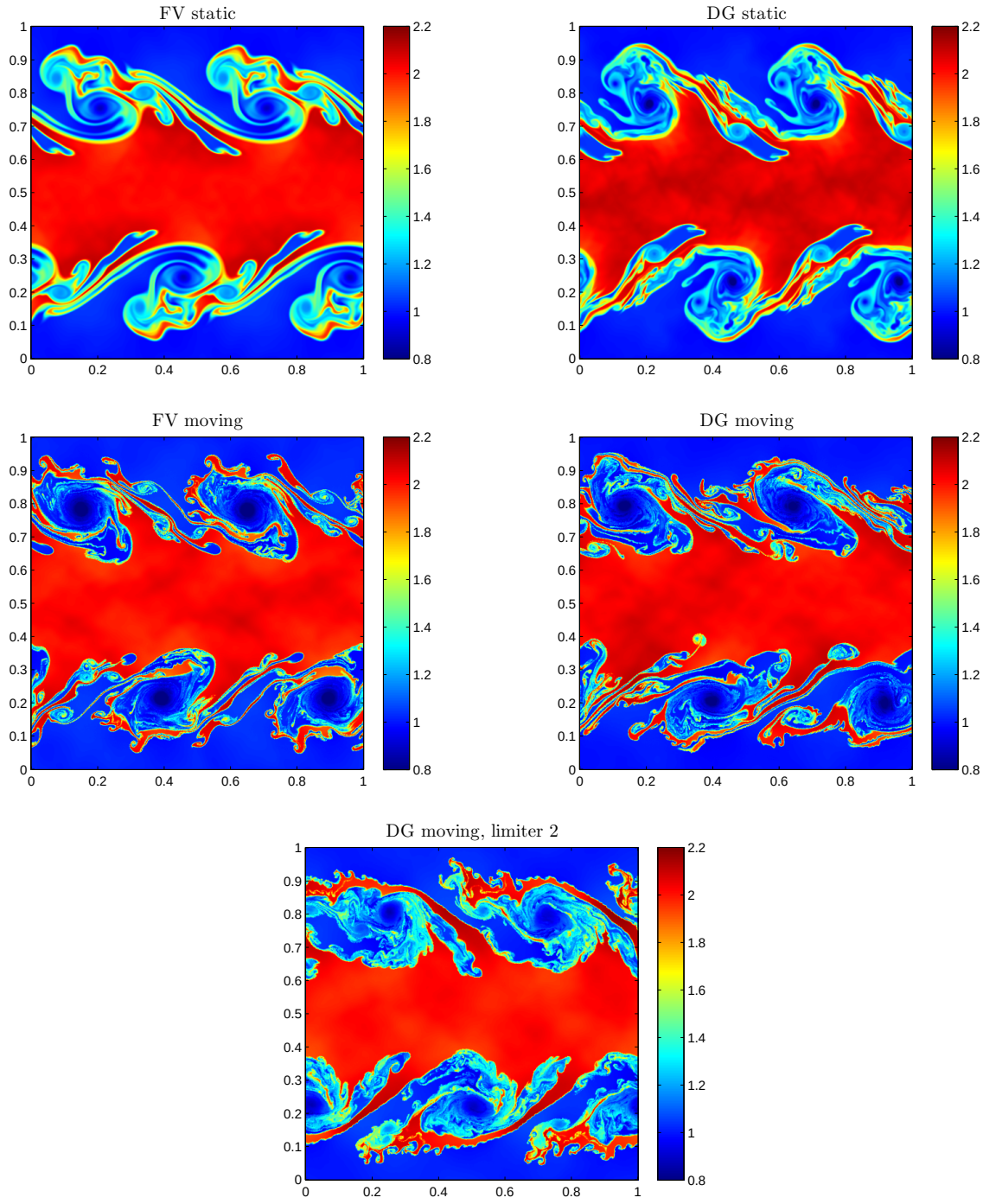

Figure 8. Kelvin Helmholtz test ($t = 2.0$, plots of density) for moving and static FV and DG methods at resolution 512^2. As in Fig. 7 we included the results of the moving DG method with the two different limiters. Variations in colour reflect the local fluid density, as indicated by the colour bars to the right of each frame.

improvement of using the DG method over a FV method is greater than the improvement of using a moving mesh over a static one.

3.7 Magnetic rotor

We now move on to testing the MHD part of the code. First we consider the magnetic rotor test (Balsara & Spicer 1999; Tóth 2000). The setup of this problem is as follows. A dense rotating disc of fluid is tapered off into the ambient fluid, which is at rest. The computational domain is a periodic box of side length 1. The adiabatic index of the gas is $\gamma = 5/3$. The initial conditions are given by $p = 0.5$, $B_x = 2.5/\sqrt{4\pi}$, $B_y = 0$,

$$\rho = \begin{cases} 10 & \text{if } r \leq r_0 \\ 1 + f & \text{if } r_0 < r \leq r_1 \\ 1 & \text{if } r > r_1 \end{cases} \tag{35}$$

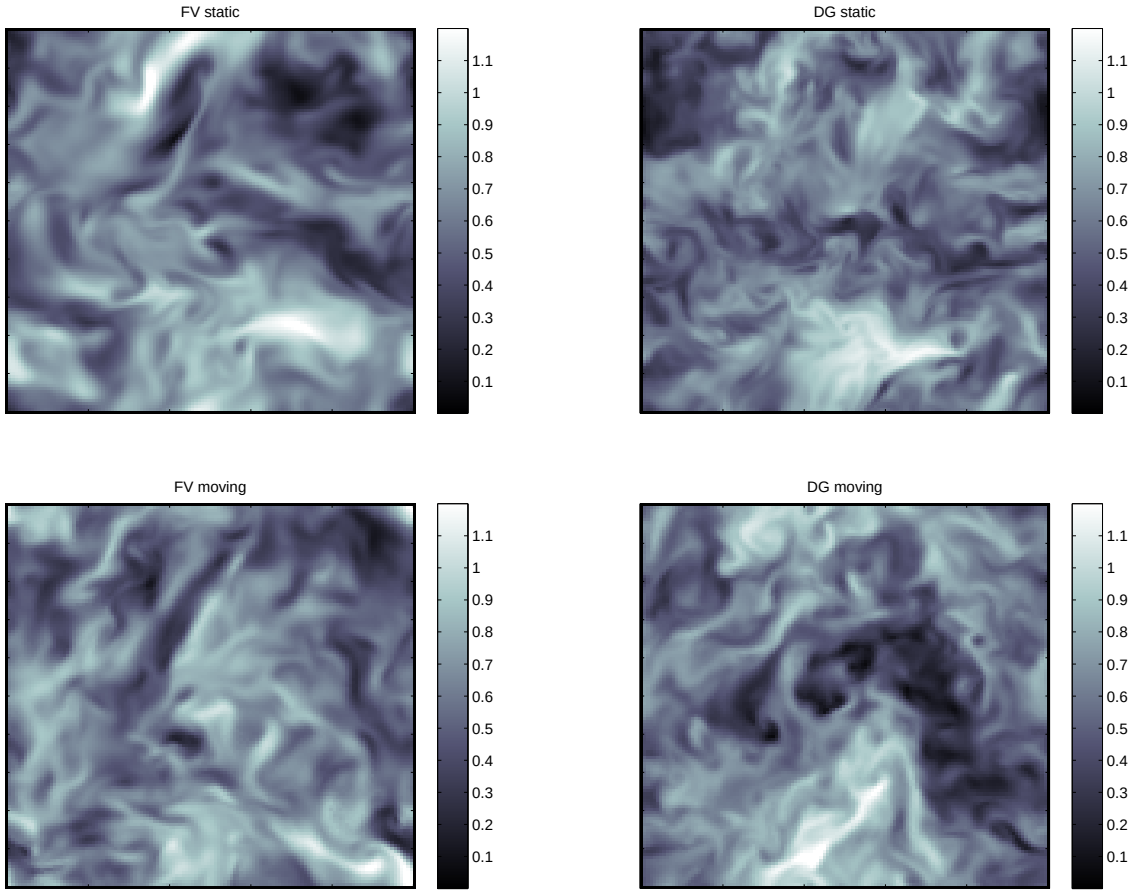

Figure 9. Plots of a slice of the velocity magnitudes $|\mathbf{v}|$ in subsonic turbulently driven isothermal gas at $t = 25.6$ for static and moving FV and DG methods in a 3D periodic box (resolution 128^3).

$$v_x = \begin{cases} -(y-0.5)/r_0 & \text{if } r \le r_0 \\ -f(y-0.5)/r & \text{if } r_0 < r \le r_1 \\ 0 & \text{if } r > r_1 \end{cases}, \tag{36}$$

$$v_y = \begin{cases} (x-0.5)/r_0 & \text{if } r \le r_0 \\ f(x-0.5)/r & \text{if } r_0 < r \le r_1 \\ 0 & \text{if } r > r_1 \end{cases}, \tag{37}$$

where $r_0 = 0.1$, $r_1 = 0.115$, $f = (r_1 - r)/(r_1 - r_0)$, $r^2 = (x-0.5)^2 + (y-0.5)^2$. In the rotor problem, centrifugal forces are not balanced so in the evolution the magnetic field confines the rotating dense fluid into an oblate rotor shape.

The rotor problem can be a sensitive test for unphysical features that occur if the global divergence of the magnetic field is not sufficiently well-constrained. Balsara & Spicer (1999); Tóth (2000); Li & Shu (2005) find that the Mach number $M = |\mathbf{v}|/c$, where $c = \sqrt{\gamma p/\rho}$ is the sound speed, can suffer serious unphysical distortions around the central rotating area.

We show a zoom-in of the Mach number at the centre of the rotor in Fig. 11, evolved with several of our schemes. No obvious unphysical artifacts are present in any of the simulations. The static mesh results show better-resolved features with some finer structures. This is due to the fact that in the moving mesh simulations, the mesh generating points move with the flow and there is actually a below-average density of mesh generating points in the center of the rotor, reducing the effective resolution in the zoom-in portion of the figure. In principle, this could be overcome by allowing local refinement of the mesh. In Fig. 12 we show the global divergence errors of the magnetic field, and the divergence errors in each cell are presented in Fig. 13. Even though the divergence errors did not have a drastic impact on the solution, methods that minimize them provide greater stability for solving arbitrary MHD problems. In the figure we see that the DG methods more tightly constrain the global divergence errors. In particular, the static DG method is the most successful one at reducing the global divergence errors and, in fact, does not require a cleaning scheme. It is followed by the moving DG method (which currently does require a Powell cleaning algorithm owing to the choice of limiter). The moving FV Powell method is third best, followed by the static Powell approach, which is considerably worse at constraining divergence errors compared to the static DG method which has no cleaning applied.

3.8 Orszag-Tang vortex

As a final test, we consider the Orszag-Tang vortex (Orszag & Tang 1979), which is an excellent test of supersonic MHD turbulence. We use the initial conditions as described by Picone & Dahlburg

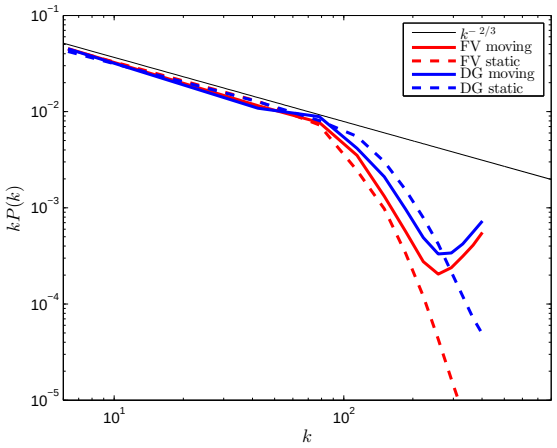

Figure 10. Velocity power spectra for the subsonic turbulently driven isothermal gas computed with the static and moving FV and DG methods. On the largest spatial scales the results display a Kolmogorov cascade ($kP(k) \propto k^{-2/3}$). The DG method does an improved job of resolving the power to smaller spatial scales for the same number of cells.

(1991):

$$\rho = \frac{\gamma^2}{4\pi}, \tag{38}$$

$$p = \frac{\gamma}{4\pi}, \tag{39}$$

$$\mathbf{v} = (-\sin(2\pi y), \sin(2\pi x)), \tag{40}$$

$$\mathbf{B} = (-\sin(2\pi y), \sin(4\pi x)). \tag{41}$$

The domain is a box of side length 1 with periodic boundaries. The gas has adiabatic index $\gamma = 5/3$. We show the results of the simulations (density distribution and local cell B field divergence errors) in Fig. 14 and Fig. 15. The static DG method (which uses no Powell cleaning) maintains minimal divergence errors which plateau quickly. This is followed by the moving DG method with Powell cleaning and thirdly the FV moving method with Powell cleaning. We also ran a static FV simulation with the Powell cleaning scheme (not shown), which became unstable due to the growth of large magnetic field divergence errors which corrupted the solution.

4 SUMMARY OF COMPARISON TO THE FINITE VOLUME APPROACH

On a static mesh, the DG formulation has clear advantages over the FV formulation. Our tests show a significant reduction of errors and angular momentum diffusion, and increased effective resolution which better characterizes small-scale fluid instabilities and recovers a Kolmogorov-like power law for turbulent cascade to smaller scales. In addition, the locally divergence-free representation of the magnetic field allows the MHD equations to be solved in a robust and stable manner without large global divergence errors. No magnetic field cleaning scheme is required in this case.

The DG method on a moving mesh also shows improvement over its FV counterpart in every test we performed. Numerical errors, angular momentum diffusion, and post-shock oscillations are reduced and the capability of resolving turbulence on small scales is enhanced. The advantages of DG over FV in our moving mesh formulation are not always as great as for the static mesh case because we had to employ a modified slope limiter to prevent unphysical oscillations. We suspect that refined limiters would allow us to more fully exploit the advantages of DG over FV, which we leave for future work.

4.1 Memory consumption and CPU time

The DG method does require greater memory usage and more CPU time than the FV approach. In our own implementation, the memory allocated to store local cell variables (fluid variables, fluid variable gradients, volumes, moments) is increased by 40 per cent for 3D simulations (for both the static and moving cases) due to the fact that in the DG method we require the second-order moments of cells in addition to their volumes and we also store moment-averaged derivative quantities $\mathbf{R}_e$ in addition to primitive gradients. However, this results in only a small net increase in total memory consumption in our implementation (< 10 per cent). A significant portion of the total memory is dedicated to storing mesh connectivity information, which is the same for the DG and FV formulations.

The CPU usage is increased by approximately 25 per cent for static 3D DG runs and 35 per cent for moving mesh 3D runs. This is due to the fact that in the DG method we are required to perform additional steps, specifically reading gradient information in the input, writing gradient information at every snapshot, calculating second-order cell moments with Gaussian quadrature in addition to cell volumes, calculating flux update terms for the moment-averaged gradient quantities at every timestep, and converting these gradients to primitive gradients. For astrophysical applications that require self-gravity, the actual penalty in CPU consumption of the DG approach relative to the FV method will be significantly less than this.

5 STRENGTHS OF THE DG METHOD IN ASTROPHYSICAL CONTEXTS

The second-order DG method developed here shows improvements in accuracy over the second-order FV MUSCL-Hancock approach without significant increase in computation time or memory consumption. The procedure is readily compatible with hierarchical time stepping and mesh refinement. The performance of our DG method on simple test problems suggest that it would improve simulations of cosmological structure formation such as those performed with AREPO (e.g. Kereš et al. (2012); Torrey et al. (2012); Nelson et al. (2013); Vogelsberger et al. (2013)).

The locally divergence-free representation of the magnetic field in the DG method reduces global divergence errors in $\nabla \cdot \mathbf{B}$. It is desirable to use this DG representation of the solution in cases where CT is not applicable. Such is the case for a moving mesh, where it is presently unclear whether the CT approach can be adapted to an evolving unstructured mesh. The locally divergence-free DG technique improves the current FV Powell scheme used in AREPO to solve the MHD equations (Pakmor & Springel 2012). The method would be useful in studying, for example, the potentially important role magnetic fields play in accretion processes and explosions (e.g. Duffell & MacFadyen (2011, 2012, 2013), where the moving mesh formulation is needed to minimize large advection errors from bulk flows (Genel et al. 2013).

The DG method can be generalized to provide higher order

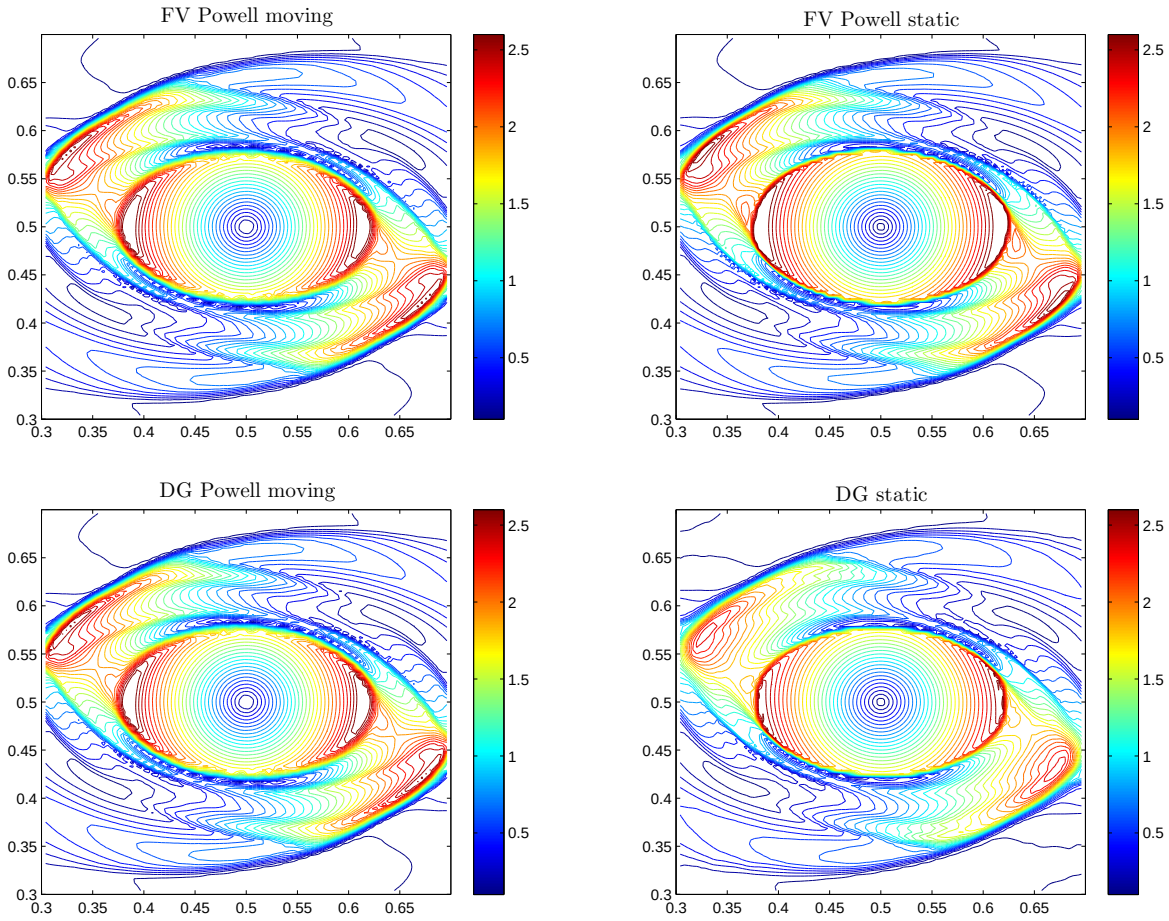

Figure 11. Contour plots of Mach number in magnetic rotor at $t = 0.295$ (resolution 512^2) shown for static and moving FV methods with Powell cleaning, moving locally divergence-free DG method with Powell cleaning, and static locally divergence-free DG method without cleaning. The simulations do not exhibit numerical artifacts typical of some MHD solvers that employ cleaning schemes. The static locally divergence-free DG method does not require Powell cleaning. Owing to our current choice of limiter for the moving DG approach, which takes a weighted average of local and stencil-determined gradients, we require Powell cleaning in this case.

accuracy on arbitrary meshes and does not adversely affect the parallelizability of current fluid solvers because cells continue to communicate with only their nearest neighbours. In this case, a higher order time stepping scheme, such as Runge-Kutta, would be preferable, to maintain the same order of accuracy in both the space and time domain.

Finally, we note that the DG method we have implemented shows significant reduction of errors and angular momentum diffusion compared to the FV method. It could play an important role in improving the current generation of AMR codes.

6 IMPROVING THE SLOPE LIMITER IN FUTURE WORK

We find that our moving DG formulation is sensitive to the choice of slope limiter and we cannot use the same slope limiter as we do for the static DG and moving and static FV method described in Springel (2010). In addition to capturing shock discontinuities, this limiter identifies and limits smooth extrema and produces unphysical oscillations in the solution. Our proposed alternate limiter, designed as a very simple WENO-type limiter, works well and pro-

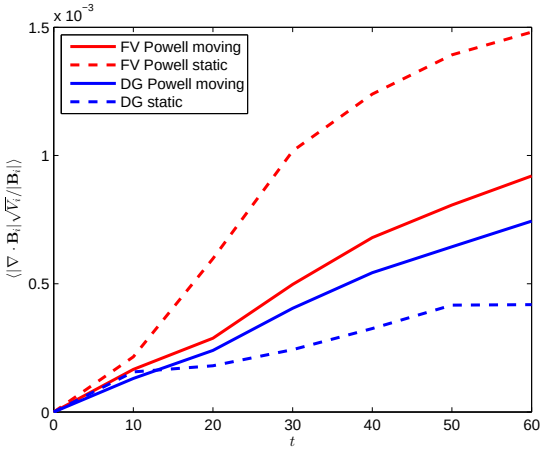

Figure 12. Analysis of the global divergence of the magnetic field for the four methods presented in Fig. 11 for the magnetic rotor problem. The DG methods demonstrate a better handling of the global divergence errors, owing to their locally divergence-free formulation.

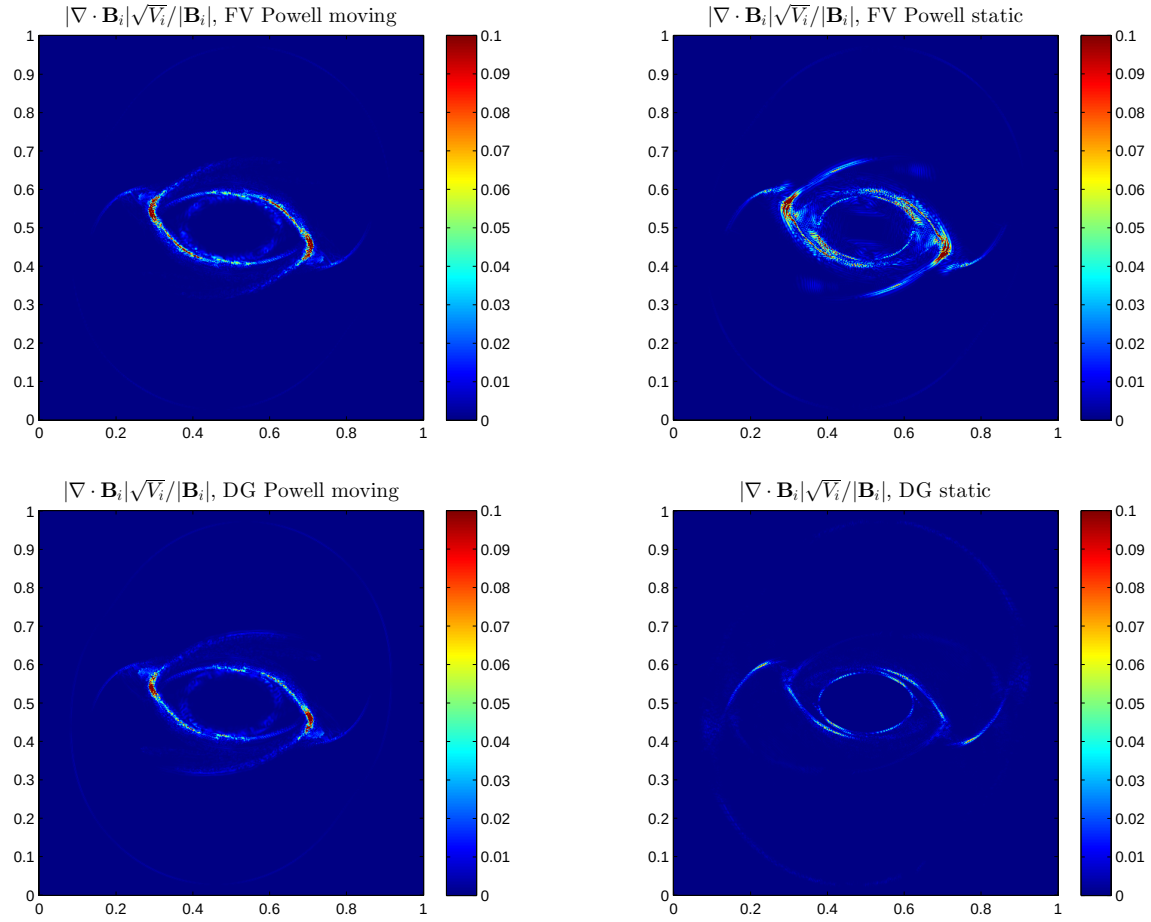

Figure 13. Divergence errors in the magnetic field for magnetic rotor test corresponding to the plots in Fig. 11.

vides stable results. However some of the advantages gained by DG over FV are not as great as in the static mesh case owing to our choice of limiter, and so an investigation for more refined limiters is clearly a priority for future efforts. WENO and Hermite WENO type approaches (Luo, Baum & Löhner 2007) seem to be a promising avenue to explore. These limiters replace solution polynomials with reconstructed polynomials of the same order of accuracy which also preserve cell averages (hence are fully conservative).

7 CONCLUDING REMARKS

We have presented a new numerical procedure for solving the fluid and MHD equations on moving and static meshes based on the DG method. The technique is an attractive and competitive alternative to the predominant FV approaches used in astrophysics. The DG scheme we developed, which is based on the centroidal Taylor basis expansion in each cell, is in fact a generalization of the FV method, where local gradients (and higher order derivatives in general) are evolved just like fluid variables, instead of using a stencil to estimate their values. In this way, gradients are purely local. The second-order DG procedure we developed does not significantly increase the runtime of the simulations compared to the FV approach. The DG method can also be readily extended to higher-order while keeping inter-element communications minimal (elements only communicate with adjacent elements with a common face), unlike FV schemes. This allows for higher-order DG codes to be highly parallelizable. In addition, the DG formulation is well-suited for unstructured meshes and mesh refinement strategies, since the method is compact (the representation of the solution on each element is independent).

On static meshes, second-order DG techniques demonstrate superior accuracy over the same-order FV method. Particularly striking is the reduction of angular momentum diffusion. As a result, DG schemes could reduce the disadvantage Eulerian codes have compared to SPH (which conserves angular momentum, but has difficulties in other areas such as resolving fluid instabilities). Moreover, in the DG formulation the magnetic field can be represented in a locally divergence-free form, which leads to a stable scheme for solving the MHD equations without the need of a cleaning scheme. The method shows superior control of global B-field divergence errors over the Powell cleaning scheme. Of course, CT schemes are preferred whenever possible because they restrict the divergences of magnetic fields to zero to machine precision. However, it is presently unknown how to extend the CT procedure to arbitrary meshes or to arbitrary hierarchical time stepping schemes. The locally divergence-free DG method is therefore seen to have possible applications in AMR simulations with adaptive highly flexible, hierarchical time stepping, required for large-scale cosmological runs.

On moving meshes, our DG method also shows improvement over the FV approach. A challenge with the DG formulation on

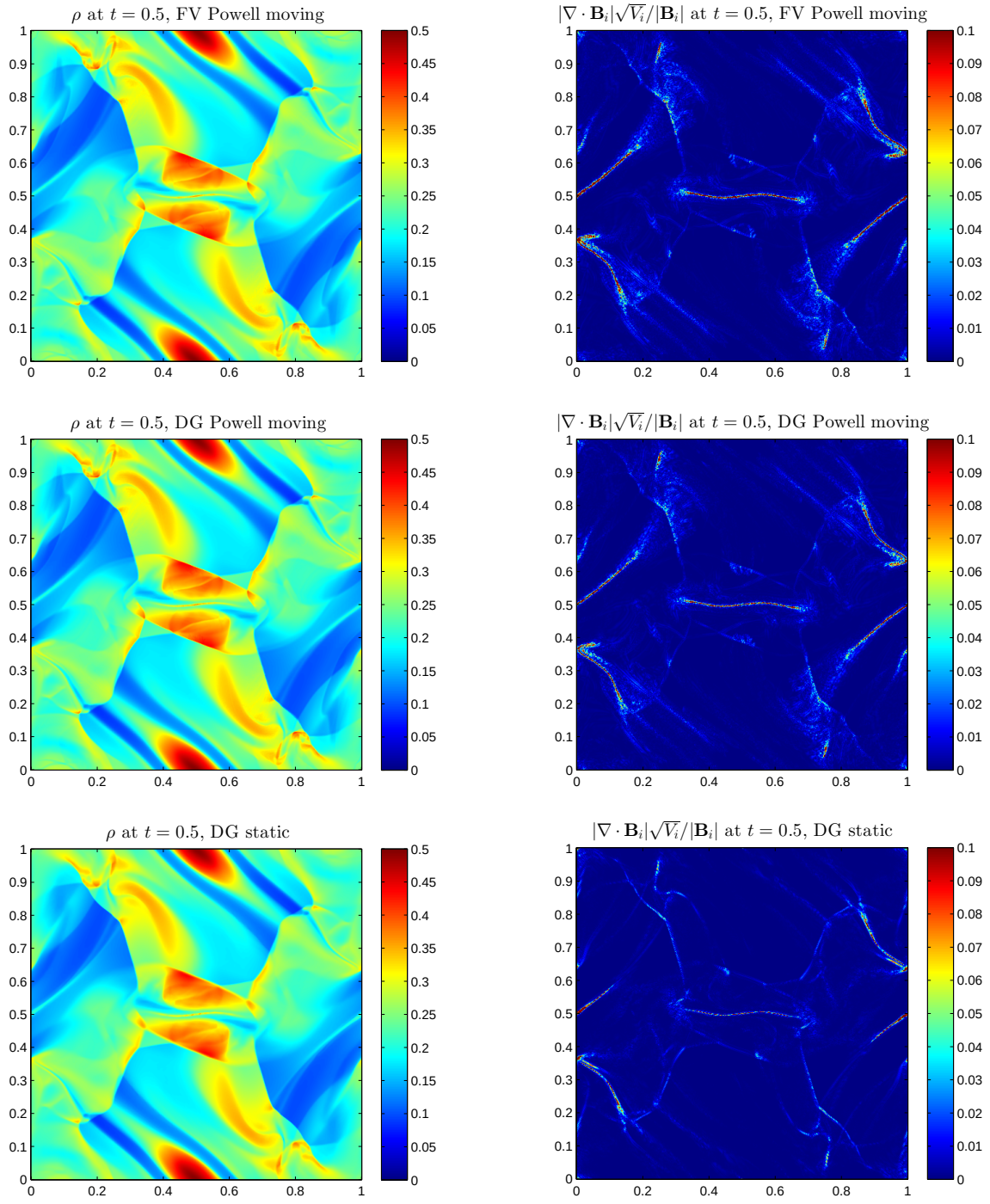

Figure 14. Plots of density and local divergence errors in the Orszag-Tang test at $t = 0.5$ (resolution 512^2) for moving FV method with Powell cleaning, moving locally divergence-free DG method with Powell cleaning, and static locally divergence-free DG method without cleaning, as labelled above each frame. All simulations do a reasonable job of arriving at an artifact-free solution. The static FV method with Powell cleaning (not shown) performs poorly and its solution becomes corrupted by local divergence errors.

moving meshes is that the solution can be sensitive to the choice of slope limiter, and we cannot use the same limiter as we do for DG on a static mesh. Performing slope limiting on a cell at a local minimum or local maximum can produce unphysical oscillations in the DG gradient solutions. To prevent this, we have currently implemented a slope limiter that takes a weighted (by an oscillation factor) average of the local DG unlimited slope and the slope obtained by a stencil (projected onto a divergence-free basis in the case of magnetic fields). This allows our method to be stable, and decreases convergence errors, post-shock oscillations, and angular momentum diffusion as well as enhancing resolution for describing turbulence given a fixed number of cells. These improvements already make the new procedure desirable over the FV approach. But we have not yet maximally exploited all the advantages of the DG

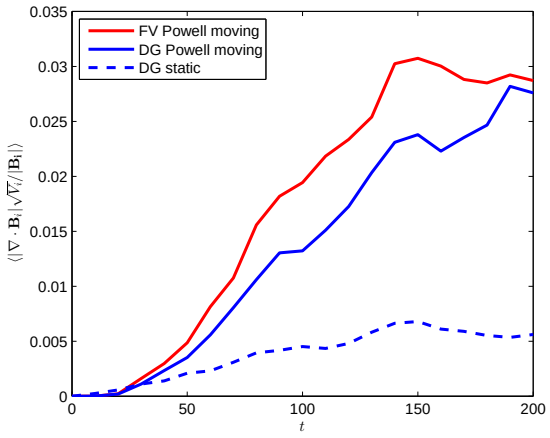

Figure 15. Analysis of the global divergence of the magnetic field for the three methods presented in Fig. 14 for the Orszag-Tang test. The DG methods demonstrate a better constraint on the global divergence errors, owing to their locally divergence-free formulation.

scheme as suggested by the comparison of the DG and FV methods on a static mesh. We do still require a Powell cleaning scheme for MHD simulations (on moving meshes only) since our gradients are a combination of the DG gradients and stencil gradients. Even so, we reduce global divergence errors compared to moving mesh FV simulations, which helps promotes the stability of MHD simulations on moving meshes. Further refinements to the DG method on a moving mesh and an exploration of different limiters form the basis for future work in this area.

The significant advantages and desirable features the centroidal Taylor-basis DG method offers over the FV approach can lead to improvements in grid-based astrophysical simulations, even at the second-order level of accuracy. The numerical results we present indicate the potential of the DG method to be a competitive procedure for large-scale astrophysical problems.

ACKNOWLEDGMENTS

This material is based upon work supported by the National Science Foundation Graduate Research Fellowship under Grant No. DGE-1144152. Any opinion, findings, and conclusions or recommendations expressed in this material are those of the authors(s) and do not necessarily reflect the views of the National Science Foundation. The simulations in this paper were run on the Odyssey cluster supported by the FAS Science Division Research Computing Group at Harvard University. PM would like to thank V. Springel, D. Muñoz, D. Nelson, and P. Torrey for useful discussions about the AREPO code architecture. LH acknowledges support from NASA grant NNX12AC67G. MV acknowledges support from NASA through Hubble Fellowship grant HST-HF-51317.01.

REFERENCES

Balsara D. S., 2001, Journal of Computational Physics, 174, 614
Balsara D. S., Spicer D. S., 1999, Journal of Computational Physics, 149, 270
Bassi F., Rebay S., 1997a, J. Comput. Phys., 131, 267
—, 1997b, J. Comput. Phys., 138, 251
Bauer A., Springel V., 2012, MNRAS, 423, 2558
Cockburn B., Li F., Shu C.-W., 2004, J. Comput. Phys., 194, 588
Dedner A., Kemm F., Kröner D., Munz C.-D., Schnitzer T., Wesenberg M., 2002, Journal of Computational Physics, 175, 645
Duffell P. C., MacFadyen A. I., 2011, ApJS, 197, 15
—, 2012, ApJ, 755, 7
—, 2013, ArXiv e-prints
Evans C. R., Hawley J. F., 1988, ApJ, 332, 659
Fromang S., Hennebelle P., Teyssier R., 2006, A&A, 457, 371
Fryxell B. et al., 2000, ApJS, 131, 273
Genel S., Vogelsberger M., Nelson D., Sijacki D., Springel V., Hernquist L., 2013, ArXiv e-prints
Ghostine R., Kesserwani G., Mos R., Vazquez J., Ghenaim A., 2009, International Journal for Numerical Methods in Fluids, 59, 423
Gresho P. M., Chan S. T., 1990, International Journal for Numerical Methods in Fluids, 11, 621
Hernquist L., Katz N., 1989, ApJS, 70, 419
Hoteit H., Ackerer P., Mos R., Erhel J., Philippe B., 2004, International Journal for Numerical Methods in Engineering, 61, 2566
Hui W. H., Li P. Y., Li Z. W., 1999, Journal of Computational Physics, 153, 596
Kereš D., Vogelsberger M., Sijacki D., Springel V., Hernquist L., 2012, MNRAS, 425, 2027
Li F., Shu C.-W., 2005, J. Sci. Comput., 22-23, 413
Liska R., Wendroff B., 2003, SIAM J. Sci. Comput., 25, 995
Luo H., Baum J. D., Löhner R., 2007, J. Comput. Phys., 225, 686
—, 2008, J. Comput. Phys., 227, 8875
Miniati F., Martin D. F., 2011, ApJS, 195, 5
Miyoshi T., Kusano K., 2005, Journal of Computational Physics, 208, 315
Muñoz D. J., Springel V., Marcus R., Vogelsberger M., Hernquist L., 2013, MNRAS, 428, 254
Nelson D., Vogelsberger M., Genel S., Sijacki D., Kereš D., Springel V., Hernquist L., 2013, MNRAS, 429, 3353
Orszag S. A., Tang C.-M., 1979, Journal of Fluid Mechanics, 90, 129
O'Shea B. W., Bryan G., Bordner J., Norman M. L., Abel T., Harkness R., Kritsuk A., 2004, ArXiv Astrophysics e-prints
Pakmor R., Bauer A., Springel V., 2011, MNRAS, 418, 1392
Pakmor R., Springel V., 2012, ArXiv e-prints
Picone J. M., Dahlburg R. B., 1991, Physics of Fluids B, 3, 29
Powell K. G., Roe P. L., Linde T. J., Gombosi T. I., de Zeeuw D. L., 1999, Journal of Computational Physics, 154, 284
Price D. J., 2012, Journal of Computational Physics, 231, 759
Rasio F. A., Shapiro S. L., 1991, ApJ, 377, 559
Sijacki D., Vogelsberger M., Kereš D., Springel V., Hernquist L., 2012, MNRAS, 424, 2999
Springel V., 2005, MNRAS, 364, 1105
—, 2010, MNRAS, 401, 791
Stone J. M., Gardiner T. A., Teuben P., Hawley J. F., Simon J. B., 2008, ApJS, 178, 137
Toro E., 1999, Riemann Solvers and Numerical Methods for Fluid Dynamics.: A Practical Introduction., Applied mechanics: Researchers and students. Springer-Verlag GmbH
Torrey P., Vogelsberger M., Sijacki D., Springel V., Hernquist L., 2012, MNRAS, 427, 2224
Tóth G., 2000, J. Comput. Phys., 161, 605
van Leer B., 1974, Journal of Computational Physics, 14, 361
Vogelsberger M., Genel S., Sijacki D., Torrey P., Springel V., Hernquist L., 2013, ArXiv e-prints

Vogelsberger M., Sijacki D., Kereš D., Springel V., Hernquist L., 2012, MNRAS, 425, 3024
Wadsley J. W., Stadel J., Quinn T., 2004, NA, 9, 137

This paper has been typeset from a TEX/ LATEX file prepared by the author.